International Conference on Multiphase Flow, ICMF'98
Lyon, France, June 8-12, 1998

Numerical Analysis of Particle Motion in Turbulent Channel Flow

Toru MIZUYA and Nobuhide KASAGI

Department of Mechanical Engineering
The University of Tokyo
Hongo 7-3-1
Bunkyo-ku, Tokyo 113-8656
Japan

Abstract

The behavior of dispersed particles in turbulent channel flow was investigated by using direct numerical simulation (DNS). The particle-to-fluid density ratio ρ_p/ρ_f is changed to be 1.05, 8.0 and 713, whilst the relaxation time τ_p^+ 3 and 7. Among various dynamical effects acting on each particle, the drag force, the added mass effect, the pressure gradient of flow and the Saffman lift force are taken into account. The interaction between fluid turbulence and particle motion is treated by either one-way or two-way coupling method.

It is observed that the turbulence intensity is slightly changed by the dispersed particles in spite of their low volume fraction $\phi_v \sim 10^{-6}$, but the relative magnitudes of the forces acting on particles are not predicted much differently in one-way and two-way coupling computations. In all cases simulated, the drag is found to play a dominant role, while the added mass effect remains minor. In the case of $\rho_p/\rho_f = 1.05$, the pressure gradient effect is also significant. When $\rho_p/\rho_f = 713$, the accumulation of particles into the near-wall low-speed streaks is observed regardless of the particle relaxation time, and it is found that the drag effect should be mainly responsible for this phenomenon.

1. Introduction

Particle-laden turbulent flows are common in natural and industrial processes and it is important to understand the characteristics of the particle motion in fluid turbulence, especially in wall turbulence from both engineering and environmental viewpoints. With the recent development of computers and numerical techniques, direct numerical simulations (DNSs) have been applied to various types of turbulent flows. DNSs of particle-laden turbulent flows have also been carried out (see, McLaughlin (1994) and Crowe (1996)).

It is known that the fluid turbulence is modulated by the presence of dispersed particles (see, e.g., Gore & Crowe, 1989), and some of the previous simulations have been carried out by taking into account the two-way interaction between fluid and particles (Elghobashi & Truesdell, 1993; Squire & Eaton, 1990; Pan & Banerjee, 1996, 1997). However, in most of the simulations of particle-laden turbulent flows, the reactive effect of dispersed particles on fluid turbulence is neglected, so that one-way coupling method is adopted. In addition, it is assumed in many previous studies that only drag and gravitational forces act on particles, though it is known that particles in fluid turbulence are driven also by other forces such as lift, pressure gradient and added mass effect.

As for the lift force due to the shear of fluid flow, McLaughlin (1989) and Squire & Wang (1996a) have clarified an important effect of the Saffman lift force on the deposition of heavy particles in the viscous sublayer. In the case of solid-gas two-phase flow, the drag and gravitational forces are known to play major roles as mentioned by Stock (1995). Little attention, however, has been given to this argument in the case of solid-liquid two-phase flow. Recently, Sato *et al.*(1997) made an experimental measurement of the forces acting on particles in a vertical channel flow. They have shown that the drag and gravitational forces are main contributors, and that when the particle-to-fluid density ratio is nearly equal to unity the pressure gradient and viscous stress can also be significant.

For developing a reliable numerical prediction method which is applicable to particle-laden wall turbulence, it is very much helpful to know when and how each force acting on a particle would be of primary significance. Hence, the objective of the present work is to investigate further various dynamical effects on particles and the resultant particle behavior near a solid wall via DNSs of the particle-laden turbulent flow in a plane channel.

2. Numerical Procedure

The flow geometry and coordinate system are shown in Fig. 1. The fluid flow in a plane channel

is described by the continuity and Navier-Stokes equations. They are given in the following dimensionless forms,

$$\frac{\partial u_i^*}{\partial x_i^*} = 0, \tag{1}$$

$$\frac{\partial u_i^*}{\partial t^*} + u_j^* \frac{\partial u_i^*}{\partial x_j^*} = -\frac{\partial p^*}{\partial x_i^*} + \frac{1}{Re_\tau} \frac{\partial^2}{\partial x_j^* \partial x_j^*} u_i^* + f_i^*, \tag{2}$$

where the variables with superscript * are those normalized by the channel half width δ and the wall friction velocity $u_\tau = \sqrt{\tau_w/\rho}$. The last term of Eq. (2), f_i^*, represents the reactive force by particles.

In the present work, the above set of governing equations of fluid motion are solved by using the pseudo-spectral method with Fourier series in the $x-$ and $z-$directions and Chebychev polynomial expansion in the $y-$direction (Kim *et al.*, 1987; Kuroda *et al.*, 1995). The ordinary no-slip boundary condition is imposed on the fluid velocity components at the walls and the periodic boundary conditions are used in the $x-$ and $z-$directions. The Reynolds number based on δ and u_τ is prescribed as $Re_\tau = 150$. The number of the spectral modes used is $64 \times 49 \times 64$ in the $x-$, $y-$ and $z-$directions, respectively. This number is not sufficiently large, but it still offers an opportunity to study major dynamical mechanisms of particle-turbulence interaction.

The trajectory of each particle is computed by integrating the equation of particle motion numerically. To do this, we use the equation proposed for $Re_p < 173$ by Mei (1994). Since this equation includes no term representing a lift force due to the flow shear, we introduce the so-called Saffman lift force. Thus, the equation of particle motion used in the present study takes the following form,

$$\begin{aligned}\frac{dv_i^*}{dt^*} = & -\frac{3}{4}\frac{\rho_f}{\rho_p}\frac{C_D}{d^*}|\vec{v}^* - \vec{u}^*|(v_i^* - u_i^*) + \frac{\rho_f}{\rho_p}\frac{Du_i^*}{dt^*} \\ & + \frac{1}{2}\frac{\rho_f}{\rho_p}\left(\frac{Du_i^*}{dt^*} - \frac{dv_i^*}{dt^*}\right) + F_{Li}^*. \end{aligned} \tag{3}$$

Each of the terms on the right hand side of Eq. (3) is the drag, the fluid pressure gradient and viscous stress, the added mass term, and the Saffman lift force, respectively. The last term of F_{Li}^* is formulated as:

$$F_{Li}^* = 1.615 \frac{6}{\pi}\frac{\rho_f}{\rho_p}\frac{1}{d^*}\sqrt{\frac{1}{Re_\tau}}\frac{\dfrac{\partial u_1^*}{\partial y^*}}{\left|\dfrac{\partial u_1^*}{\partial y^*}\right|^{1/2}}(u_1^* - v_1^*)\delta_{i2}, \tag{4}$$

by McLaughlin (1989) and Wang & Squire (1996a). The drag coefficient of C_D is given as,

$$C_D = \begin{cases} \dfrac{24}{Re_p}(1 + 0.15 Re_p^{0.687}) & (Re_p \le 800), \\ 0.43 & (\text{otherwise}), \end{cases} \tag{5}$$

with the particle Reynolds number Re_p defined as:

$$Re_p = \frac{|\vec{v} - \vec{u}|d}{\nu} = Re_\tau d^* |\vec{v}^* - \vec{u}^*|. \tag{6}$$

Note that moving particles are not necessarily located at the numerical grid points where the fluid velocity is calculated, so we have to estimate it at each particle position and each time step. For this purpose, the cubic spline interpolation is adopted (Yeung & Pope, 1988).

The influence of dispersed particles on the fluid flow is implemented as a source term f_i in Eq. (1). This term is introduced only in two-way coupling simulation. Presently, f_i is extrapolated to eight grid points, which form the control volume containing the particle by using volume-weighted averages (Squire, 1990).

The present conditions of dispersed particles are summarized in Table 1, where d^+, $\tau_p^+ (\equiv \rho_p (d^+)^2/18\rho_f)$ and ϕ_v are the diameter, relaxation time and volume fraction of particles, respectively. Superscript + denotes the normalization with u_τ and ν. Particles P1 and P2 correspond to those of polystyrene in water and of steel in water, respectively, whilst both P3 and P4 correspond to olive oil droplets in the atmosphere. The total number of particles dispersed in the computational volume is 64800. Initially, particles are distributed uniformly in space in a fully developed turbulent field, and each particle is assumed to have a velocity, which is equal to the local fluid velocity at the same position. For Particle P1, only one-way coupling simulation is carried out, whereas both one-way and two-way coupling simulations are done for Particles P2, P3 and P4. The collision between the wall and particles is assumed to be inelastic, but frictionless (Pedinotti *et al.*, 1992).

The value of integral time step Δt^+ is set to 0.24 and the total steps of the computation is 6000. The statistics of particle motion are calculated by ensemble averaging over the period of $t^+ = 960 - 1440$.

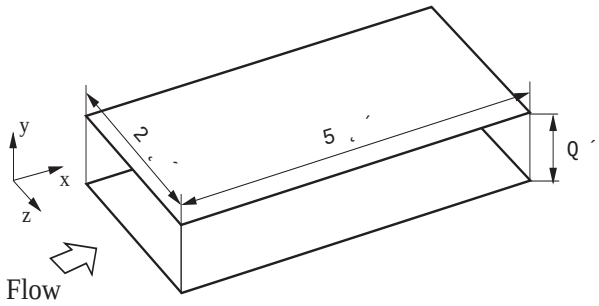

Figure 1: Computational domain and coordinate system.

Table 1: Particle conditions.

Particle	ρ_p/ρ_f	d^+	τ_p^+	ϕ_v
P1	1.05	7.17	3	1.88×10^{-2}
P2	8.0	2.59	3	8.84×10^{-4}
P3	713	0.275	3	1.05×10^{-6}
P4	713	0.42	7	3.77×10^{-6}

3. Results and discussion

3.1. Statistics of fluid turbulence and particle motion

The mean and fluctuating velocity components in particle-laden turbulent flows are shown in Figs. 2 and 3. The two-way coupling treatment would not be necessary under the present condition of ϕ_v according to Elghobashi (1991). It is seen, however, in the present two-way coupling computation that the flow field is discernibly affected by the dispersed particles. The turbulence intensity in the streamwise direction is slightly enhanced by the particles near the wall, and that in the wall-normal direction becomes larger around the center of the channel. Though it is known that small particles tend to decrease the turbulence intensity, whilst large particles enhance it, such a fact is not evident in the present study.

Figure 4 shows the mean wall-normal component of the particle velocity. It is found that the velocities of P1 and P2 are almost equal to zero, so that a stationary state has been reached, while those of P3 and P4 are still in a transient state moving toward the walls. Figure 5 shows the distribution of the mean particle Reynolds number Re_p, which takes maximum and minimum values near the wall and around the channel center, respectively. It is confirmed that the assumption of $Re_p < 173$ for Eq. (3) is well satisfied in the present study. The distribution of the particle concentration is shown in Fig. 6. All particles but particle P1 ($\rho_p/\rho_f = 1.05$) show a tendency to concentrate near the wall; this tendency is more pronounced in the case of particles with larger τ_p and ρ_p/ρ_f.

Figure 7 summarizes the root-mean-square velocity fluctuations of particle motion. It is evident that the rms fluctuations near the wall are larger in the $x-$ direction and smaller in the $y-$ and $z-$ directions than those of fluid turbulence. This fact is in good agreement with the recent results of LES of Wang & Squire (1996b). The difference between the results obtained by the one-way and two-way coupling simulations seems to be minor, although it is clearly discernible.

3.2. Forces acting on particles

Each term acting on a particle in Eq. (3) has been calculated in the present simulations, and the averaged streamwise and wall-normal components are shown in Figs. 8 and 9, respectively.

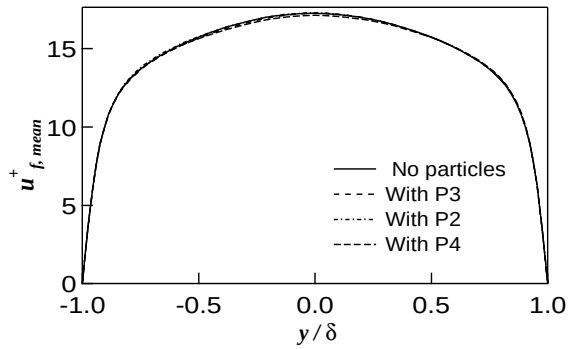

Figure 2: Mean velocity profiles of fluid flow with particles.

(a) Streamwise component

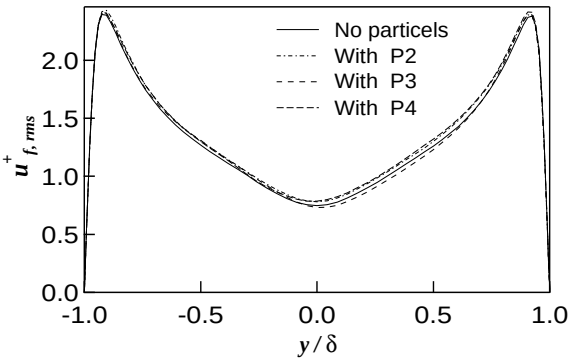

(b) Wall-normal component

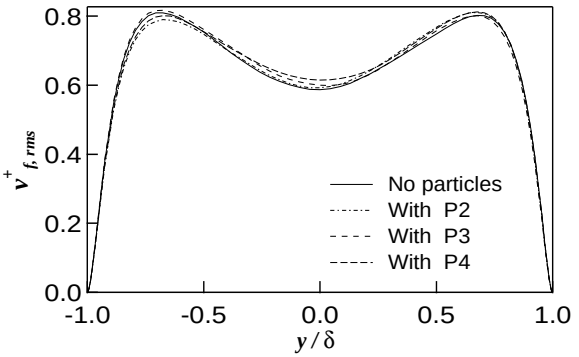

(c) Spanwise component

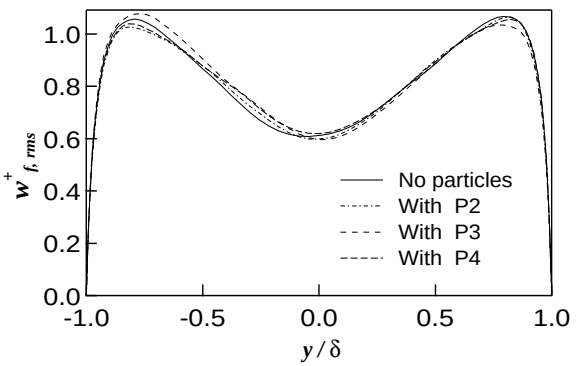

Figure 3: RMS velocity fluctuations of fluid flow with particles; (a) $u_{f,rms}$, (b) $v_{f,rms}$, and (c) $w_{f,rms}$.

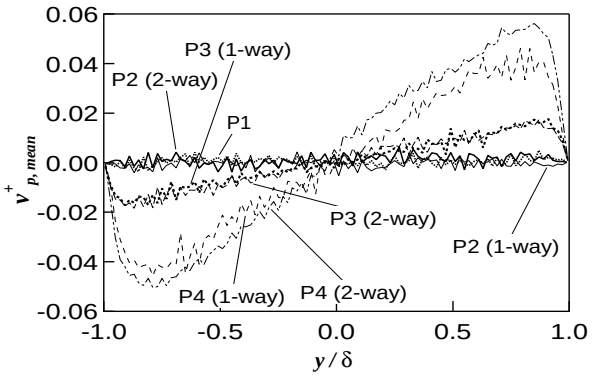

Figure 4: Averaged wall-normal components of particle velocity

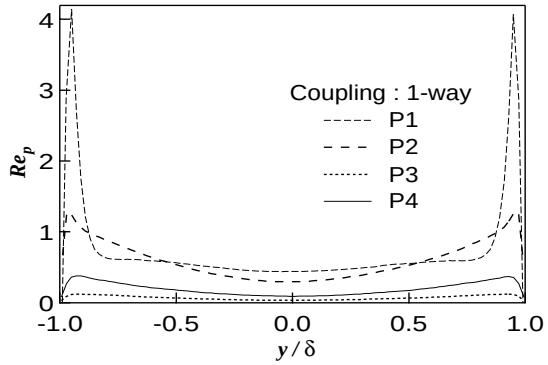

Figure 5: Averaged particle Reynolds numbers.

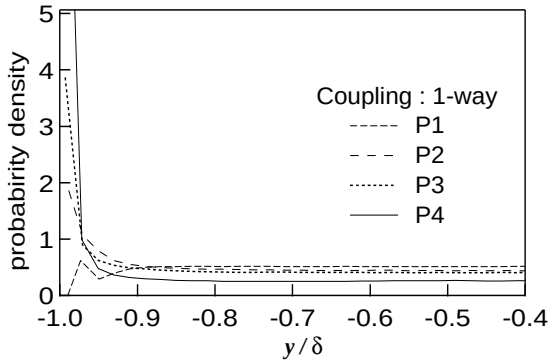

Figure 6: Distributions of particle concentrations.

(a) Particle P1

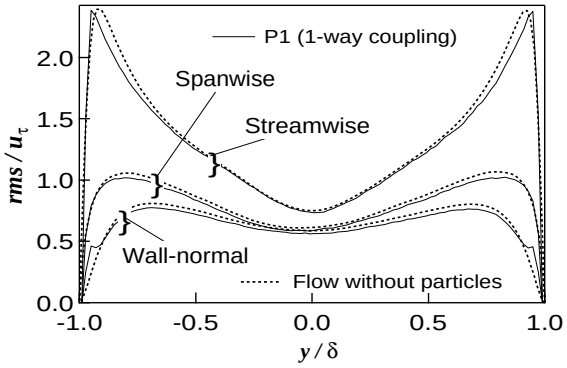

(b) Particle P2

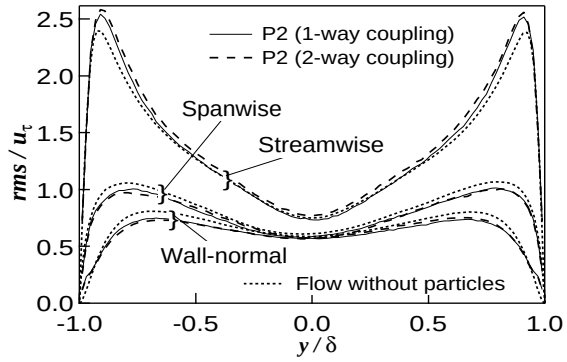

(c) Particle P3

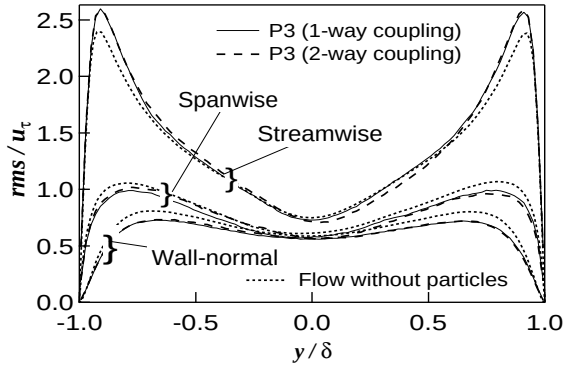

(d) Particle P4

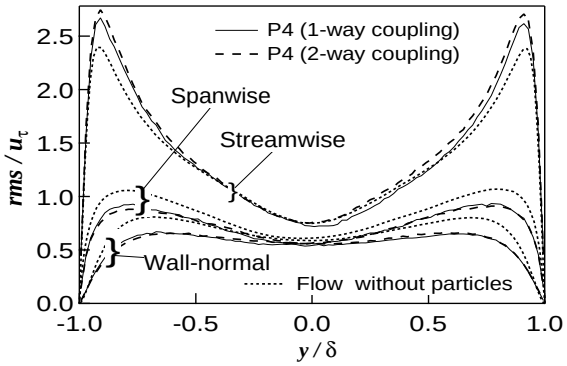

Figure 7: RMS velocity fluctuations of particles; (a) P1, (b) P2, (c) P3 and (d) P4.

The results for various particles as well as those obtained by the one-way and two-way coupling methods are compared each other. From these figures, it is found that the drag is a main force in all cases, whereas the added mass effect is very weak except for P1, of which density ratio is $\rho_p/\rho_f = 1.05$. It is also evident that the one-way and two-way coupling simulations give almost the same results (see, e.g., Figs. 8(b) and (c)). For Particles P3 and P4 of $\rho_p/\rho_f = 713$, the Saffman lift force in the wall-normal component is additionally significant in the near-wall region. Moreover, for Particle P2 of $\rho_p/\rho_f = 8.0$, the role of the lift force becomes even more important and the force due to the fluid pressure gradient also exhibits its effect near the wall.

For P1 of $\rho_p/\rho_f = 1.05$, the pressure gradient effect is one of the primary forces and this fact is in good agreement with Sato *et al.* (1997). In the wall-normal direction, the drag, lift and pressure gradient have comparable effects near the wall, whilst the force due to fluid pressure gradient is dominant in the rest of the channel cross section. These three forces show the opposite sign in contrast to other cases. Since the Saffman lift force working on particle P1 tends to push particles away from the wall, the particle concentration decreases in the near-wall region as shown in Fig. 6. This fact, however, is contrary to the common knowledge that particles in wall turbulence tend to concentrate into the near-wall region. The reason is likely because we have not applied the wall-correction to the drag coefficient of particles (McLaughlin, 1994) and underestimated it in the near-wall region.

3.3. Preferential concentration of particles in turbulent channel flow

In Fig. 10, an instantaneous near-wall distribution of particles at $0.97 < y/\delta < 0.99$ for each particle condition is shown along with the gradation contour of streamwise fluid velocity at $y/\delta = 0.98$. The area visualized is $5\pi\delta \times 2\pi\delta$ in the $x-$ and $z-$directions, respectively. In Fig. 10(d), Particle P4 clearly tends to concentrate into the low-speed streaks. This preference can also be observed for Particle P3 in Fig. 10(c) although it is weaker, but can not be confirmed for Particles P1 and P2 in Figs. 10(a) and (b). By comparing these facts with the results in Figs. 8 and 9, it is concluded that the drag force should be a main cause of the particle accumulation into the low-speed streak.

It is also found that, since the increase of τ_p^+ is accompanied with the decrease in the drag, particles with larger τ_p^+ are more likely to exhibit preferential concentration. According to the result by Wang and Squire (1996b), particles with larger τ_p^+ show more accumulation when $\tau_p^+ \leq 117$, but the opposite trend is observed when $\tau_p^+ > 117$. The present result is in conformity with their observation. Note that this preferential concentration of particles is limited to a very thin region in the close vicinity of the wall and that it has not been observed even in the region of $0.93 < y/\delta < 0.96$ in all cases.

From comparison between Figs. 10(b) and (c), it is found that, if the particles have the same τ_p^+, those with larger ρ_p/ρ_f show more degree of accumulation. In addition, since the other forces act oppositely for the particles with smaller ρ_p/ρ_f as shown in Figs. 8(a) and 9(a, b, c), they play a role of preventing the particles from forming preferential concentration.

In Fig. 11, the near-wall distributions of particles are shown with the instantaneous pressure fluctuation at $y/\delta = 0.98$. Although the effect of fluid pressure gradient is significant for Particle P1 as shown in Figs. 8(a) and 9(a), any substantial correlation between the particle concentration and pressure distribution cannot be observed. This confirms again that the drag force is a primary cause of preferential concentration of particles near the wall.

4. Conclusions

The one-way and two-way coupling DNSs of particle-laden turbulent flow in a channel were performed. The following conclusions are derived:

(1) Although the volume fraction ϕ_v assumed presently is very low ($\sim 10^{-6}$), the flow field is slightly affected by the interaction with the dispersed particles.

(2) The particles, which have been introduced uniformly into the initial flow field, tend to concentrate toward the wall except those with $\tau_p^+ = 3$ and $\rho_p/\rho_f = 1.05$. This tendency is more marked with increasing τ_p^+ and ρ_p/ρ_f.

(3) The velocity fluctuations of particle motion are larger in the streamwise direction and smaller in the wall-normal and spanwise directions than those of fluid turbulence. The difference between the statistics of particle motion obtained by the one-way and two-way coupling simulations appears minor, although it is clearly discernible.

(4) For the particles of $\rho_p/\rho_f = 713$, the drag is dominant over the whole channel cross section and the effect of lift force appears only near the wall. In the case of $\rho_p/\rho_f = 8.0$, the effect of pressure gradient and the lift force become appreciable near the wall, although the drag is still dominant. When the density ratio decreases even more to $\rho_p/\rho_f = 1.05$, the drag, pressure gradient and lift reach comparable magnitudes near the wall, whilst the pressure gradient effect is dominant in the rest of the channel cross section.

(5) The particles of $\tau_p^+ = 7$ and $\tau_p^+ = 3$ with $\rho_p/\rho_f = 713$ show a tendency to concentrate into the low-speed streaks; this is mainly owing to the drag force.

The authors thank Professor S. Banerjee at UC Santa Barbara for his valuable discussions during

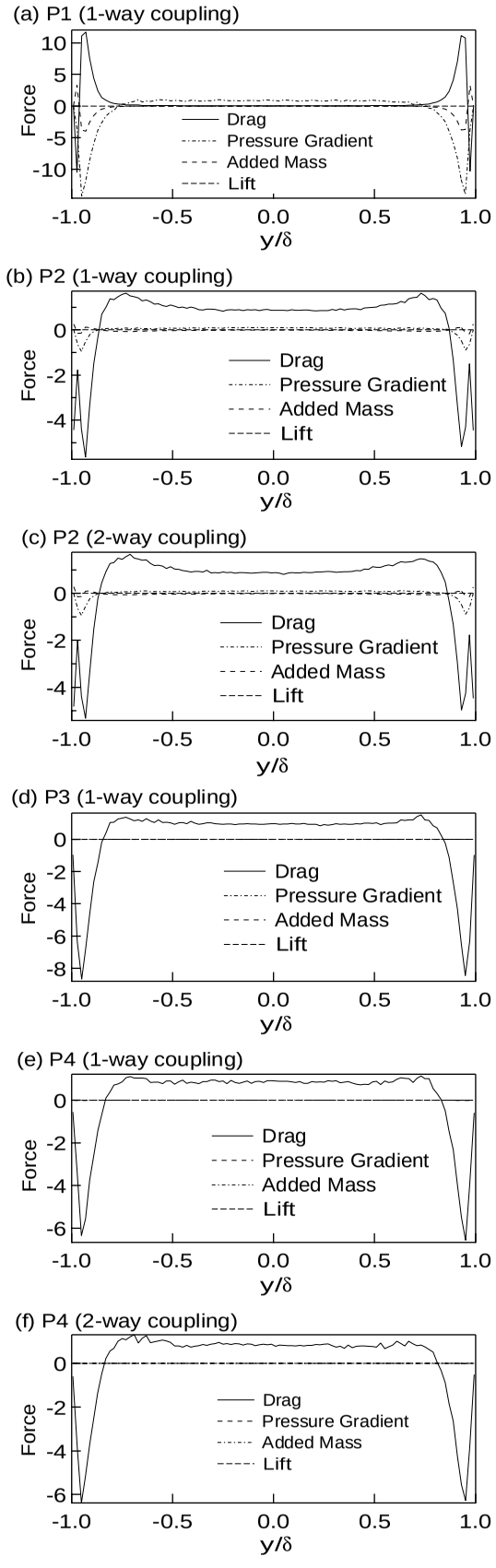

Figure 8: Streamwise components of the force acting on particles

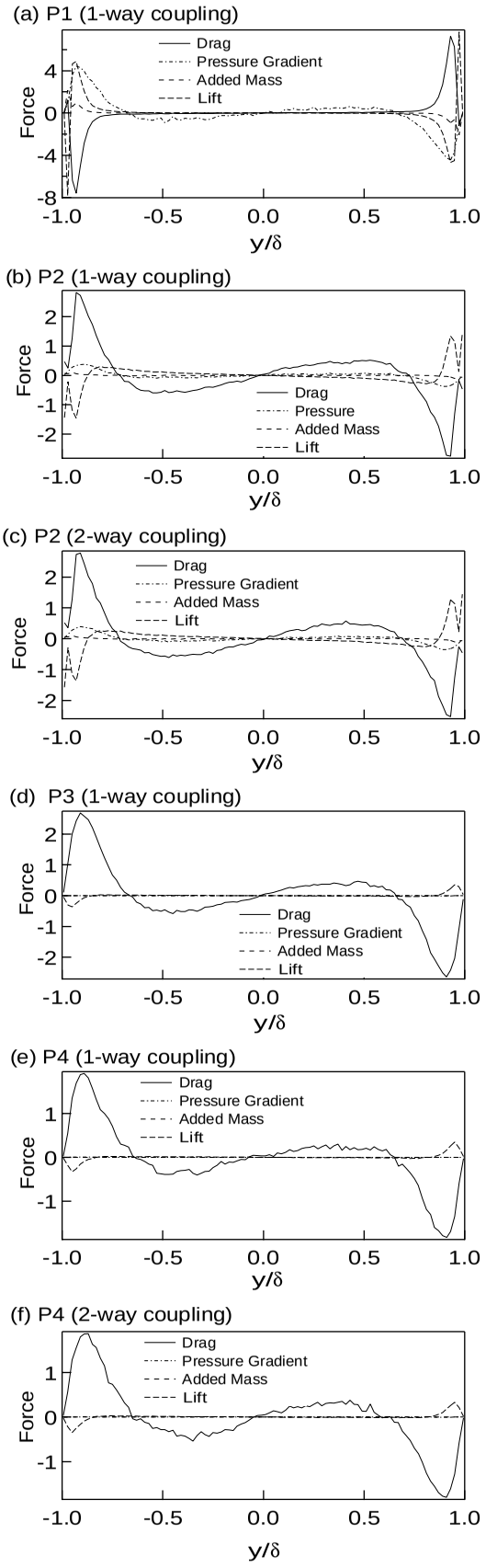

Figure 9: Wall-normal components of the force acting on particles

$\Longrightarrow$ Flow

(a) P1(one-way coupling)

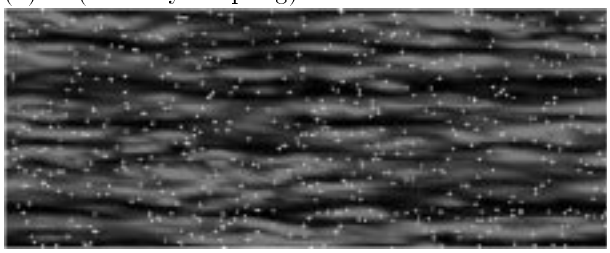

(b) P2(one-way coupling)

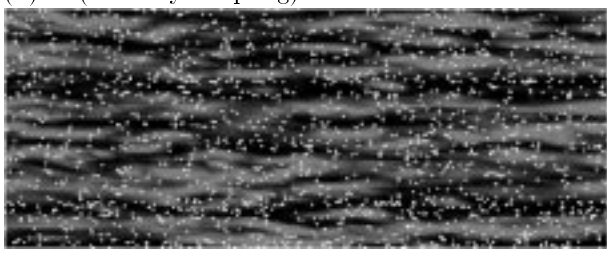

(c) P3(one-way coupling)

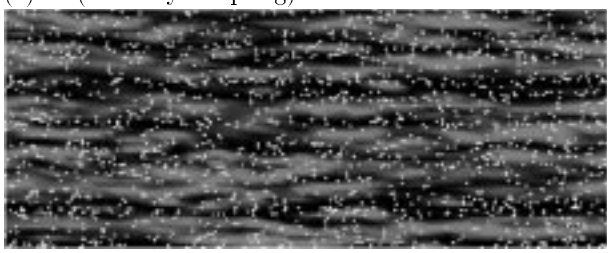

(d) P4(one-way coupling)

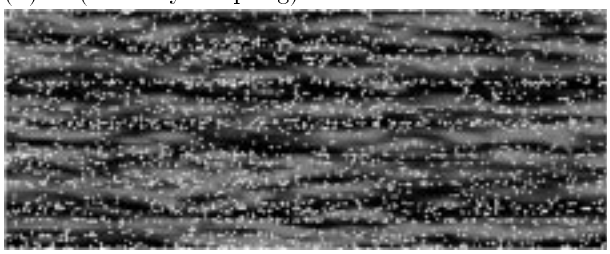

Figure 10: Particle distribution in $0.97 < y/\delta < 0.99$ and instantaneous field of streamwise fluid velocity fluctuation at $y/\delta = 0.98$. White points correspond to dispersed particles. Black to light gray: $u_f^{'+} = -1.1$ to 1.1.

$\Longrightarrow$ Flow

(a) P1(one-way coupling)

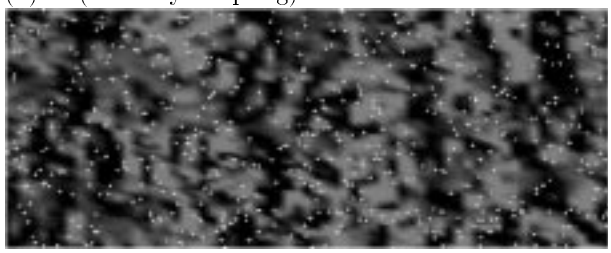

(b) P2(one-way coupling)

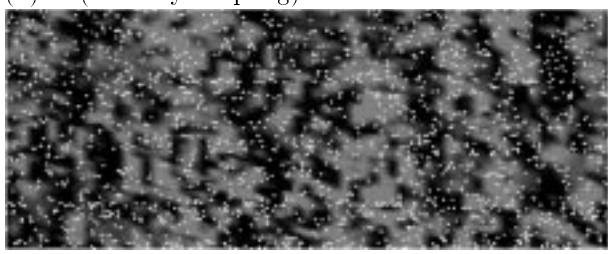

(c) P3(one-way coupling)

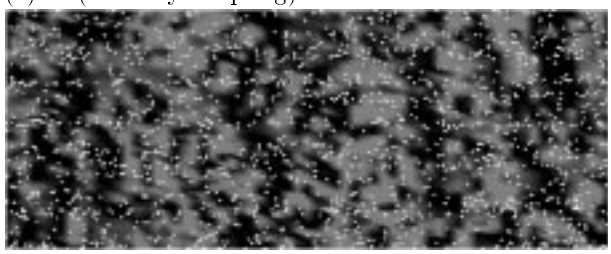

(d) P4(one-way coupling)

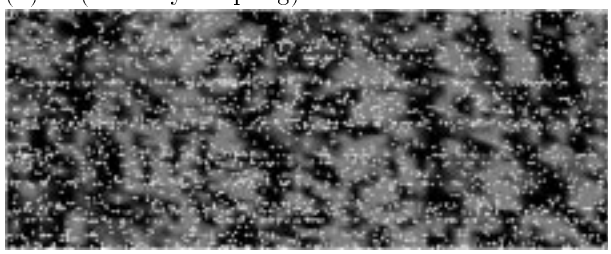

Figure 11: Particle distribution in $0.97 < y/\delta < 0.99$ and instantaneous field of pressure fluctuation at $y/\delta = 0.98$. White points correspond to dispersed particles. Black to light gray: $p^{'+} = -1.1$ to 1.1.

the course of this work. This work was supported by the Ministry of Education, Science and Culture through the Grant-in-Aid for Scientific Research (B) (No. 08455102).

References

Crowe, C. T., Troutt, T. R. and Chung, J. N. 1996 Numerical model for two-phase turbulent flows. *Ann. Rev. Fluid Mech.* **28**, 11-43.

Gore, R. A. and Crowe, C. T. 1989 Effect of particle size on modulating turbulent intensity. *Int. J. Multiphase Flow* **15**, 279-285.

Eaton, J. K. and Fessler, J. R. 1994 Preferential concentration of particles by turbulence. *Int. J. Multiphase Flow* **20**, Suppl., 169-209.

Elghobashi, S. E. & Truesdell, G. C. 1993 On the two-way interaction between homogeneous turbulence and dispersed solid particles. 1: Turbulence modification. *Phys. Fluids* **5**, 1790-1801.

Elghobashi, S. E. 1991 Particle-laden turbulent flows: direct simulation and closure model. *Appl. Sci. Res.* **52**, 301-314.

Kim, J., Moin, P. & Moser, R. 1987 Turbulent statistics in fully developed channel flow at low Reynolds number. *J. Fluid Mech.* **177**, 133-166.

Kuroda, A., Kasagi, N. & Hirata, M. 1995 Direct numerical simulation of turbulent plane Couette-Poiseuille flows: Effect of mean shear rate on the near-wall turbulence structures. *Turbulent Shear Flows* **9**, Springer, 241-257.

Maxey, M. R. & Riley, J. J. 1983 Equation of motion for a small rigid sphere in a nonuniform flow. *Phys. Fluids* **26**, 883-889.

Mei, R. 1994 Flow due to an oscillating sphere and an expression for unsteady drag on the sphere at finite Reynolds number. *J. Fluid Mech.* **270**, 133-174.

McLaughlin, J. B. 1989 Aerosol particle deposition in numerically simulated channel flow. *Phys. Fluids A* **1**, 1211-1224.

McLaughlin, J. B. 1994 Numerical computation of particle-turbulent interaction. *Int. J. Multiphase Flow* **20**, Suppl., 211-232.

Pan, Y. & Banerjee, S. 1996 Numerical simulation of particle-interaction with wall turbulence. *Phys. Fluids* **8**, 2733-2755.

Pan, Y. & Banerjee, S., 1997 Numerical investigation of the effect of large particles on wall-turbulence. *Phys. Fluids* **9**, 3786-3807.

Pedinotti, S., Mariotti, G. & Banerjee, S. 1992 Direct numerical simulation of particle behavior in the wall region on turbulent flows in horizontal channels. *Int. J. Multiphase Flow* **18**, 927-941.

Sato, Y., Hayashi, I. & Hishida, K. 1997 Lagrangian statistics of fluid/particle correlated motion in channel flow. *Proc. 11th Symp. Turbulent Shear Flows, Grenoble*, P24.11-16.

Squire, K. D. & Eaton, J. K. 1990 Particle response and turbulence modification in isotropic turbulence. *Phys. Fluids A* **2**, 1191-1203.

Stock, D. E. 1995 Particle dispersion in turbulent gas flows. *Proc. 2nd Int. Conf. on Multiphase Flow, Kyoto*, PL2.1-13.

Wang, Q. & Squire, K. D. 1996a Large eddy simulation of particle deposition in a vertical turbulent channel flow. *Int. J. Multiphase Flow* **22**, 667-683.

Wang, Q. & Squire, K. D. 1996b Large eddy simulation of particle-laden turbulent channel flow. *Phys. Fluids* **8**, 1207-1223.

Yeung, P. K. and Pope, S. B. 1988 An algorithm for tracking fluid particles in numerical simulations of homogeneous turbulence. *J. Comput. Phys.* **79**, 373-416.